arXiv:1210.1337v1 [cond-mat.mtrl-sci] 4 Oct 2012

Unusual magnetism of layered chromium sulfides $M\mathrm{CrS}_2$ ($M =$ Li, Na, K, Ag, and Au)

A. V. Ushakov,[1,2,3] D. A. Kukusta,[2,4] A. N. Yaresko,[2] and D. I. Khomskii[1]

[1] *II. Physikalisches Institut, Universität zu Köln, Zülpicherstraße 77, D-50937 Köln, Germany*
[2] *Max-Planck-Institut für Festkörperforschung, Heisenbergstraße 1, D-70569 Stuttgart, Germany*
[3] *Institute for theoretical physics, Clausthal University of Technology, Leibnizstraße 10, D-38678 Clausthal Zellerfeld, Germany*
[4] *Institute for Metal Physics, 36 Vernadskyi Bld., UA-03680 Kiev, Ukraine*

$M\mathrm{CrS}_2$ compounds ($M =$ Li, Na, K, Cu, Ag, and Au) with triangular Cr layers show large variety of magnetic ground states ranging from 120° antiferromagnetic order of Cr spins in LiCrS_2 to double stripes in AgCrS_2, helimagnetic order in NaCrS_2, and, finally, ferromagnetic Cr layers in KCrS_2. On the base of *ab-initio* band structure calculations and an analysis of various contributions to exchange interactions between Cr spins we explain this tendency as originating from a competition between antiferromagnetic direct nearest-neighbor d–d exchange and ferromagnetic superexchange via S p states which leads to the change of the sign of the nearest neighbor interaction depending on the radius of a M ion. It is shown that other important interactions are the third-neighbor interaction in a layer and interlayer exchange. We suggest that strong magneto-elastic coupling is most probably responsible for multiferroic properties of at least one material of this family, namely, AgCrS_2.

PACS numbers: 71.20.Lp, 71.70.Gm, 75.30 Et

I. INTRODUCTION

Frustrated magnetic systems attract now considerable attention.[1] Among them there are systems with very strong geometric frustrations (e.g. kagome or pyrochlore systems), and also less frustrated ones – e.g. systems with triangular lattices. Triangular magnets are overconstrained and most often they display one or the other type of magnetic ordering. Nevertheless, frustrated nature of triangular layers strongly influences their magnetic properties, often making them rather unusual and very sensitive to small variations of the electronic and lattice structure.[2] Such materials also present definite practical interest, e.g., as possible thermopower materials[3] or new multiferroics.[4,5]

The presence of orbital degeneracy may introduce special features in the properties of triangular magnets, see e.g., Ref. 6. But even without such degeneracy, as in materials containing half-filled d-(sub)shells (Fe^{3+} d^5; Cr^{3+} t_{2g}^3), the properties of such systems can be rather nontrivial.

Contrary to similar materials with oxygen instead of sulfur, $M\mathrm{CrS}_2$ compounds are much less studied. But it was recently shown that at least some of them, such as AgCrS_2, show very interesting behavior: this particular material belongs to a pyroelectric class, below the Néel temperature $T_N = 50$ K it develops a rather unusual double-stripe (DS) magnetic order[7] and also becomes multiferroic.[8] Motivated by this findings, and trying to understand the reasons for this unusual type of magnetic ordering, apparently also relevant for the appearance of ferroelectricity, we undertook a study of this and similar systems with the M-ions Li, Na, K, Cu, Ag, Au. These systems, though in principle very similar and all containing as the main building block the same CrS_2 triangular layers, show very different magnetic ordering: from the pure nearest neighbor antiferromagnetism (120° structure) for LiCrO_2[9] with the smallest M-cation Li^+ and up to ferromagnetic (FM) CrS_2 layers in KCrS_2[10] with the largest M-ion K^+, with more complicated magnetic structures in the other systems. Our *ab-initio* and model calculations allow us to explain the general tendency of magnetic ordering in this very rich class of compounds, and this understanding may be helpful not only for these compounds, but also for other magnetic systems with triangular layers.

II. CRYSTAL AND MAGNETIC STRUCTURE

The crystal structure of $M\mathrm{CrS}_2$ series has been determined in Refs. 7, 11–14. Cr atoms form a triangular lattice within CrS_2 layers, and the latter are joined by M atoms [Fig. 1(a)]. Cr atoms are located at the center of trigonally distorted octahedra composed of sulfur ones. Each S atom is shared by three different octahedra. But the "connection" between layers is different in different compounds. In compounds with alkali metals, Li, Na, and K are also sitting in S_6 octahedra. One can visualize the structure of these compounds as originating from the rock-salt structure of (actually hexagonal) CrS, in which Cr and alkali ions are ordered in consecutive (1,1,1) planes, so that Cr as well as Li, Na, or K are octahedrally coordinated by anions (the detailed stacking of Cr, S and alkali layers maybe different).

At the same time, the structure of the systems $M\mathrm{CrS}_2$ with M=Cu, Ag, Au is different. In corresponding oxides the nonmagnetic ions Cu^{1+} and Au^{1+} with the configuration d^{10} are linearly coordinated. They are located in the centers of oxygen dumbbells, i.e., are sandwiched between two oxygens belonging to different MO_2) layers. The resulting structure is that of delafossites.[15]

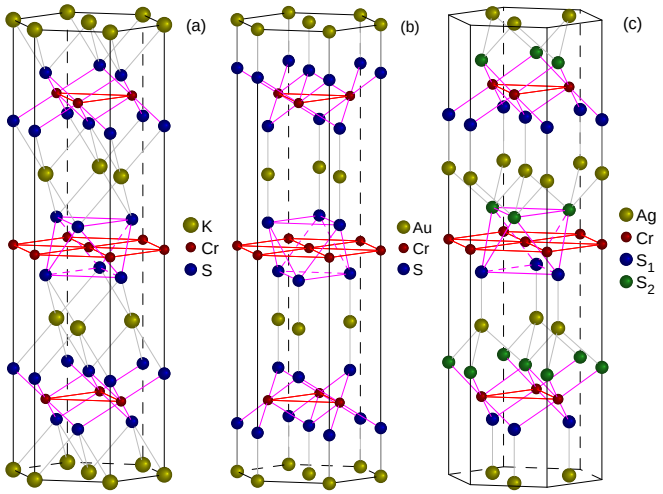

FIG. 1. (Color online) High temperature rhombohedral crystal structures of $KCrS_2$ (a), $AuCrS_2$ (b), and $AgCrS_2$ (c). Also shown is a distorted CrS_6 octahedron surrounding a Cr ion in the cell center.

The structure of their sulfur analogues is more interesting: it is "in between" that of, say, $LiCrO_2$ and $AgCrO_2$. Such M^+ ions are located on top of a S_3 triangle of one, say, the lower CrS_2 layer, but are connected by vertical bonds to one S^{2-} ion of the next, upper layer [Fig. 1(c)]. In effect Cu, Ag, and Au are in a "tripod" made of four S ions, or in the distorted (elongated in c-direction) S_4 tetrahedron. Metal ions in such S_4 tetrahedra are strongly shifted towards the upper, apical S ion. All such tripods, or tetrahedra, are pointing in the same direction, e.g., up, so that the resulting structure does not have an inversion symmetry and is of a pyroelectric class. However this interesting structural feature, though probably important for some properties of these materials, seem to play minor role in magnetic properties of these compounds, which mainly depend on interactions in CrS_2 layers. Whereas most structural studies of $MCrS_2$ with M=Cu and Ag give this structure with M-ions in sulfur "tripods" and R3m symmetry,[6] there are also reports of a different crystal structure. Thus, in the recent paper Ref. 14 it is concluded that the symmetry of $AuCrS_2$ is $R\bar{3}m$ or, maybe, $R3m$, and the actual structure is the delafossite one with linearly coordinated Au^+ [Fig. 1(b)].

$MCrS_2$ compounds have diverse magnetic structures and a broad set of physical properties. Being coupled antiferromagnetically (AFM) between the layers, they exhibit quite different in-plane ordering at low temperatures.

At high temperatures $LiCrS_2$ belongs to $P\bar{3}m1$ space symmetry group. According to neutron scattering measurements the magnetic structure of this compound below the Néel temperature $T_N = 55$ K exhibits a triangular spin arrangement (120° structure) within the triangular planes, with adjacent planes being coupled antiferromagnetically.[13,16] This structure is typical for Heisenberg antiferromagnets with nearest neighbor coupling on a triangular lattice. The observed value of Cr^{3+} spin magnetic moment equals $2.26\mu_B$, being considerably smaller than the expected value of $3\mu_B$. The difference may be presumably attributed to covalency effects, which can considerably alter the distribution of the spin density around the Cr^{3+} ion. Indeed, one can expect such behavior, keeping in mind much smaller size of Li^+ ions and respective reduction of unit cell volume.

$KCrS_2$ undergoes AFM transition at $T_N = 38$ K.[10] the symmetry group at high temperature is rhombohedral $R\bar{3}m$. The magnetic structure, in contrast to $LiCrS_2$, consists of ferromagnetic layers perpendicular to the c axis, which are antiferromagnetically coupled to adjacent ones. The paramagnetic Curie temperature of $KCrS_2$ is not low ($\theta_C = 112$ K) and indicates that the ferromagnetic interaction in the planes is the dominant one. The observed value of the Cr^{3+} spin magnetic moment ($3.04\pm0.05\mu_B$) obtained by neutron scattering[10] is in good agreement with the expected value of $3\mu_B$ and with the value obtained from the susceptibility measurements ($3.1\mu_B$). This can be interpreted as an indication that in $KCrS_2$ covalency effects are relatively weak.

In contrast to $LiCrS_2$ and $KCrS_2$, $AgCrS_2$ undergoes at $T_N = 41.6$ K a first-order phase transition from a paramagnetic rhombohedral $R3m$ structure to an antiferromagnetic monoclinic Cm structure.[7] Most interesting, the material was found to be ferroelectric below T_N, i.e., it is a multiferroic system.[8] Note that this phenomenon differs from the eventual polarization of $AgCrS_2$ due to its pyroelectric crystal structure: this polarization appears only in a magnetically-ordered state and lies in the ab-plane, not along c-direction, as the eventual pyroelectric polarization due to the crystal structure itself. In addition to being ferroelectric below T_N, the low-temperature phase of $AgCrS_2$ exhibits an unconventional collinear magnetic structure that can be described as double ferromagnetic stripes coupled antiferromagnetically, with the magnetic moment of Cr^{3+} aligned along the b axis within the anisotropic triangular plane. Ferroelectricity below T_N in $AgCrS_2$ is explained as a consequence of atomic displacements at the magnetoelastically induced structural distortion, most probably driven by the double-stripe magnetic structure itself. Thus, this system can be classified as a type-II multiferroic.[4,5,17]

Similarly to $AgCrS_2$, $AuCrS_2$ undergoes a first-order magnetic and structural phase transition at $T_N = 47$ K from a paramagnetic rhombohedral $R\bar{3}m$ to a monoclinic antiferromagnetic $C2/m$ structure.[14] The simultaneous observation of magnetic and structural transition both in $AgCrS_2$ and $AuCrS_2$ gives evidence of a large magnetoelastic coupling in these systems. This coupling accounts for the stability of the observed magnetic order, considering that the structural distortions at the transition suppress the geometric frustration of the Cr layers. As we will show below, the peculiar antiferromagnetic structure observed both in $AgCrS_2$ and $AuCrS_2$ is explained by the interplay of the exchange due to direct dd hopping and that via anions (sulfur) involving nearest neighbor and

further neighbor Cr-Cr interactions, as well as the residual frustration in the triangular Cr planes.

In Table I we put different compounds in the order of increasing Cr–Cr distance, which also corresponds to an increase of a Cr–S–Cr bond angle since average Cr–S distances vary much less than the Cr–Cr ones. One immediately notices a definite correlation between the crystal structure and magnetic order: with increasing Cr–Cr distance and Cr–S–Cr angle the magnetic structure changes from the 120° AFM structure in $LiCrS_2$ with the smallest Li^+ ion and the shortest Cr–Cr distance to ferromagnetic layers in $KCrS_2$ with the largest K^+ ion and the longest Cr–Cr distance. The crossover between these limiting cases occurs via incommensurate magnetic phases in $CuCrS_2$ and $NaCrS_2$ and the double-stripe structure in $AuCrS_2$ and $AgCrS_2$. It is this correlation between crystal and magnetic structure, which is the main topic of our study. We approach this problem by performing *ab initio* calculations, in which we obtain the electronic structure of the $M\mathrm{CrS}_2$ compounds, as well as the values of relevant exchange constants. We then analyze the observed general trends in a superexchange model, discussing different relevant, often competing contributions to the total exchange.

TABLE I. Cr–Cr ($d_{\text{Cr-Cr}}$) and Cr–S ($d_{\text{Cr-S}}$) interatomic distances (in Å) as well as Cr-S-Cr bond angles θ (in degrees) for the high-temperature $M\mathrm{CrS}_2$ structures. For M=Cu and Ag only averaged $d_{\text{Cr-S}}$ is shown, while θ is given for two inequivalent S ions.

M	$d_{\text{Cr-Cr}}$	$d_{\text{Cr-S}}$	θ	magnetic structure
Li	3.4515	2.4063	91.7	AFM 120°
Cu	3.4728	2.4036	90.6, 94.6	spiral ordering
Au	3.4826	2.3862	93.7	AFM double stripes
Ag	3.4979	2.4085	92.2, 94.1	AFM double stripes
Na	3.5561	2.4249	94.3	spiral ordering
K	3.6010	2.4123	96.6	FM in plane

III. COMPUTATION DETAILS

Band structure calculations were performed using the linear muffin-tin orbitals (LMTO) method[18] as implemented in the PY-LMTO computer code.[19] We used the Perdew-Wang[20] parameterization for the exchange-correlation potential in the local spin-density approximation (LSDA). Brillouin zone integrations were performed using the improved tetrahedron method.[21]

When the spin-orbit coupling is not taken into account, the use of the generalized Bloch theorem[22] makes possible self-consistent calculations of the band structure and the total energy $E(\mathbf{q})$ for spin-spiral structures with an arbitrary wave vector $\mathbf{q}$ as described in details in Refs. 23 and 24. In these calculations the magnetization direction in an atomic sphere centered at $\mathbf{t}+\mathbf{R}$, where $\mathbf{t}$ specifies its position in a unit cell and $\mathbf{R}$ is a translation vector, is defined by two polar angles θ and $\phi = \mathbf{q}\cdot\mathbf{R} + \phi_0$. In the present work we considered only planar spin spirals with all $\theta = \pi/2$. The phase ϕ_{Cr} inside spheres surrounding Cr ions was fixed by requiring $\phi_{\text{Cr}} = \mathbf{q}\cdot\mathbf{t}_{\text{Cr}}$, whereas for all other spheres it was determined selfconsistently by diagonalizing the corresponding spin-density matrix.

This general approach allows us to treat on the same footing not only collinear, e.g., ferromagnetic or stripe, or non-collinear, e.g., 120° AFM, *commensurate* magnetic structures, but also perform calculations for *incommensurate* helical structures. The only restriction is that it should be possible to describe the magnetic structure by a single wave vector $\mathbf{q}$. After the $\mathbf{q}$ dependence of the total energy has been calculated, effective exchange interactions between Cr spins can be obtained by mapping $E(\mathbf{q})$ onto a relevant Heisenberg-like model.

The magneto-crystalline anisotropy was estimated by using the force theorem,[25] i.e., by comparing band energies obtained for selected collinear spin structures from spin-polarized relativistic calculations with the magnetization parallel to different crystallographic axes. Spin-orbit coupling in these calculations was included into the LMTO Hamiltonian at the variational step.[26]

In order to study the effect of relatively strong electronic correlations in the Cr d shell on the band structure and magnetic interaction in the $M\mathrm{CrS}_2$ compounds, for some of them we also calculated $E(\mathbf{q})$ using the rotationally invariant LSDA+U method.[27] For the double counting term the so-called atomic limit was used.[28] Other details on the implementation of the LSDA+U method in the PY-LMTO code are given in Ref. 29. Calculations were performed for the Hund's exchange coupling parameter $J = 0.9$ eV and the on-site Coulomb repulsion $U = 1.9$, 2.9, and 3.9 eV, which gives 1, 2, and 3 eV for $U_{\text{eff}} = U - J$.

IV. RESULTS AND DISCUSSION

A. Band structure and energies of different magnetic structures

Our band-structure calculations demonstrate that all atoms in $M\mathrm{CrS}_2$ compounds exhibit their valences corresponding to the stoichiometry of the compound, i.e., the atomic charges correspond to M^+, Cr^{3+}, and S^{2-}. The s orbitals of M^+ are empty, whereas the p orbital of S^{2-} are fully occupied. Since Cr atom is triply ionized, there are three d electrons localized on a Cr^{3+} ion.

The octahedral crystal field at the Cr site causes the d orbitals to split into a triplet t_{2g} (xy, xz, yz) and a doublet e_g ($3z^2 - r^2$, $x^2 - y^2$), with the energy of the t_{2g} orbitals being lower than that of the e_g states. Since there are three d electrons localized on a Cr site, in spin-restricted band structure calculations the t_{2g} states are half-filled, whereas the e_g levels are empty. In spin-polarized calculations the spin-up t_{2g} states are occupied, and spin-down t_{2g} are empty.

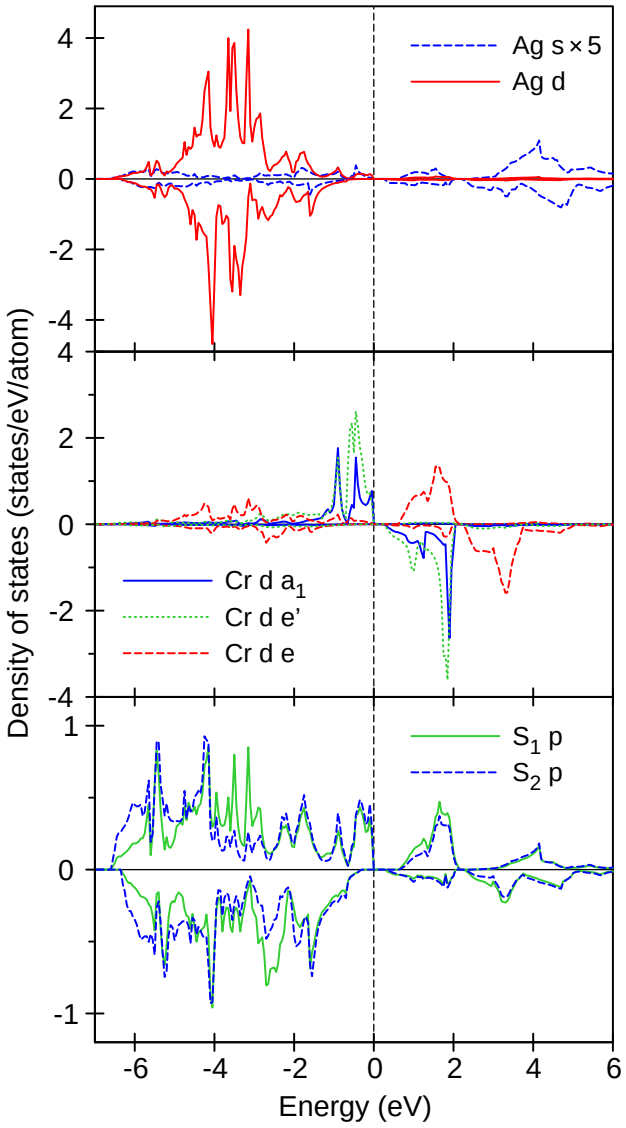

FIG. 2. (Color online) Partial densities of states in $AgCrS_2$ with the FM alignment of Cr moments. Energies are given relative to the Fermi level E_F.

The cubic component of the crystal field at the Cr site is strong enough for the t_{2g} and e_g orbitals to form two non-overlapping sub-bands separated by an energy gap of about 0.5 eV. Additional trigonal distortion along the c-axis lifts the degeneracy of the t_{2g} levels and splits them into a singlet a_{1g} and a doublet e'_g (a_1 and e' in the compounds with $R3m$ symmetry, e.g., $AgCrS_2$), which are linear combinations of the t_{2g} orbitals. Three Cr^{3+} d electrons occupy spin-up a_{1g} and e'_g orbitals.

The electronic structures and density of states (DOS) of compounds in $MCrS_2$ series are similar, so to get details specific for current calculations, we consider as an example the DOSes obtained for $AgCrS_2$ in ferromagnetic spin-polarized LSDA calculations (see Fig. 2).

The occupied part of the valence band can be subdivided into several regions. For all M-ions their valence s states are empty and d states (if they exist) are totally occupied. These valence s and d states do not contribute to the electronic density close to the Fermi-energy E_F. In $AgCrS_2$ the Ag $4d$ states appear between -6 eV and -1.5 eV.

The occupied S^{2-} $3p$ states form the broad band with the width of 6 eV between -6.5 eV and -0.3 eV, being strongly hybridized both with Ag $4d$ and Cr $3d$ states. As will be discussed later, this hybridization between Cr $3d$ and S $3p$ states is responsible for superexchange along Cr–S–Cr and Cr–S–S–Cr paths. According to our band structure calculations these materials are insulating even in the ferromagnetic state and even without including Hubbard's U. For instance for $AgCrS_2$ the LSDA gives the energy gap of 0.55 eV. That is, due to their specific electronic structure – half-filled t_{2g} subshell and empty e_g states of Cr^{3+} – they would be band insulators (in a magnetically-ordered state). When electronic correlations are accounted for in LSDA+U calculations, the occupied majority-spin t_{2g} states are shifted by $U_{\rm eff}/2$ to lower energies, whereas the unoccupied minority-spin t_{2g} and all e_g states move $\sim U_{\rm eff}/2$ to higher energies which increases the values of the gaps.

Magnetic properties and the electronic structure of $MCrS_2$ compounds are closely related to the occupancy of the Cr $3d$ states, which are spread over wide energy interval from -6 eV to 4 eV and form two non-overlapping subbands separated by energy gap. Cr e_g and t_{2g} orbitals form $pd\sigma$- and $pd\pi$-bonds with sulfur p orbitals, respectively. The hybridization between occupied Cr spin-up t_{2g} and S p-states at -1 eV and -0.5 eV is clearly observed. Being rather small below E_F, the hybridization between Cr d and S p above E_F is larger for e_g states and is well pronounced for spin-up DOSes.

Our calculations prove the clearly insulating nature of these materials. The exchange splitting $\Delta_{\rm ex} \sim 2$ eV is prominent for the Cr $3d$ bands in the whole $MCrS_2$ series where only spin-up Cr a_{1g} and e'_g orbitals are filled.

The calculated values of the Cr spin magnetic moment are close to $3\mu_{\rm B}$ for all compounds in the series. Calculations for spin spirals showed that the Cr moment depends only weakly on the wave vector of a spiral, i.e., on the kind of magnetic order. In $LiCrS_2$, for instance, the moment varies from $2.74\mu_{\rm B}$ for the 120° AFM structure to $2.98\mu_{\rm B}$ for the FM one. This also confirms the localized character of the Cr moments and suggests that magnetic interactions between them can be described by the Heisenberg model.

Damay *et al.* in Ref. 7 analyzed dynamic correlations and found a small spin gap at very low energies as $\mathbf{q} \to 0$ that has been attributed to the weak magnetic anisotropy; i.e., we conclude that the Cr spins in $MCrS_2$ are relatively isotropic and can be described by the Heisenberg model. The localized character of Cr^{3+} spin magnetic moments is confirmed in our calculations by the fact that Cr spin-up a_{1g} and e'_g states are fully occupied, localized on the Cr^{3+} site and separated from empty states by an energy gap.

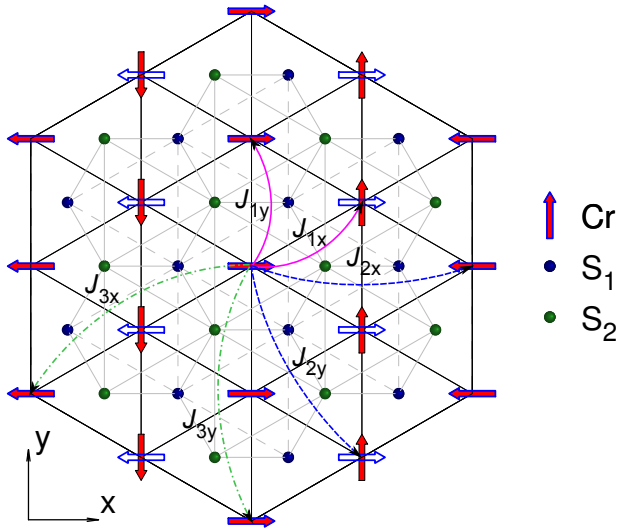

FIG. 3. (Color online) Representation of double stripe (blue arrows) and 90° (red arrows) magnetic structures within the Cr plane. One underlying (S_1) and one overlying (S_2) sulfur layers are shown as well. The low-temperature intraplane exchanges between the first (J_{1x}, J_{1y}), the second (J_{2x}, J_{2y}), and the third (J_{3x}, J_{3y}) neighbors are shown as curved lines with arrows. In the high-temperature phase $J_{1x}=J_{1y}=J_1$, $J_{2x}=J_{2y}=J_2$, $J_{3x}=J_{3y}=J_3$.

The applicability of the Heisenberg model allows us to investigate the wide range of Cr spin moment configurations within the single approach using the Heisenberg Hamiltonian in the form

$$H=\frac{1}{2}\sum_{i\neq j}J_{ij}\mathbf{S}_i\mathbf{S}_j. \tag{1}$$

Everywhere below we work in the orthogonal coordinates, choosing y-axis along one of the directions between Cr-Cr nearest neighbors in the ab-plane, and the x-axis is chosen perpendicular to it. i.e., it points from one Cr to its second neighbor, see Fig. 3. Thus, in our notation the $\mathbf{q}$-vectors of magnetic superstructures are given in these coordinates, not in the standard vectors of corresponding reciprocal lattices. We measure the in-plane components of a $\mathbf{q}$-vector in the units of $2\pi/a$ and the out-of-plane component in $2\pi/c$.

In case of an arbitrary wave vector $\mathbf{q}=(q_x,\,q_y,\,q_z)$ the Heisenberg magnetic energy in these coordinates is

$$E(\mathbf{q})=\epsilon_1(\mathbf{q})+\epsilon_2(\mathbf{q})+\epsilon_3(\mathbf{q})+\epsilon_z(\mathbf{q}) \tag{2}$$

where $\epsilon_i(\mathbf{q})$ are contribution proportional to the exchange coupling constants J_i between i-th Cr neighbors within the triangular plane (see Fig. 3). For the undistorted high-temperature (HT) rhombohedral structures

$$\epsilon_1(\mathbf{q})=J_1\left[2\cos(\sqrt{3}q_xa/2)\cos(q_ya/2)+\cos(q_ya)\right], \tag{3}$$

$$\epsilon_2(\mathbf{q})=J_2\left[\cos(q_xa\sqrt{3})+2\cos(\sqrt{3}q_xa/2)\cos(3q_ya/2)\right], \tag{4}$$

$$\epsilon_3(\mathbf{q})=J_3\left[2\cos(q_xa\sqrt{3})\cos(q_ya)+\cos(2q_ya)\right]. \tag{5}$$

An expression for interlayer coupling, $\epsilon_z(\mathbf{q})$, is particularly simple for $LiCrS_2$:

$$\epsilon_z(\mathbf{q})=J_z\cos(q_zc)\,. \tag{6}$$

In other compounds with the abc stacking of Cr layers Cr neighbors in adjacent planes sit above and below the centers of triangles, i.e., above S_1 and below S_2 positions in Fig. 3, and $\epsilon_z(\mathbf{q})$ becomes

$$\epsilon_z(\mathbf{q})=J_z\left[2\cos(q_zc/3-q_xa/(2\sqrt{3}))\cos(q_ya/2)+\cos(q_zc/3+q_xa/\sqrt{3})\right]. \tag{7}$$

When J_z is sufficiently strong it may affect in-plane magnetic order.

As sketched in Fig. 3, in the monoclinic low-temperature (LT) phases of $AgCrS_2$ and $AuCrS_2$ exchange interactions J_{nx} and J_{ny} between n-th neighbors along x and y directions are no longer equal and the expressions (3)–(5) should be modified accordingly. For instance, the energy of the nearest neighbor interaction becomes

$$\epsilon_1(\mathbf{q})=2J_{1x}\cos(q_xx_{1x})\cos(q_yy_{1x})+J_{1y}\cos(q_yy_{1y}), \tag{8}$$

where a vector $\mathbf{r}_{1x/y}$ ($x_{1x/y}$,$y_{1x/y}$,0) connects a Cr site with its nearest neighbors along x and y directions.

In order to estimate the effective exchange parameters J_i and J_z we first carried out *ab-initio* calculations for a number of $\mathbf{q}$-vectors lying in q_z=0 [Fig. 4(a)] and q_z=3/2 [Fig. 4(b)] planes. The latter value of q_z results in 180° rotation of Cr spins in adjacent layers. We then fitted the $\mathbf{q}$-dependence of the calculated total energy $E(\mathbf{q})$ (open black circles in Fig. 4) by the Heisenberg model given by (2)–(7) using a least-square fit with four (J_1, J_2, J_3, and J_z) and seven ($J_{1x,1y}$, $J_{2x,2y}$, $J_{3x,3y}$, J_z) exchange parameters for the HT and LT phases, respectively. The results of such a fit for the most interesting system $AgCrS_2$, which has the unusual double-stripe magnetic structure and becomes multiferroic below T_N, are shown in Fig. 4 by filled red circles. A good agreement between the results of the LSDA total energy calculation and of the fit proves the possibility to describe the magnetic properties of these compounds by the Heisenberg model which includes the exchange coupling constants between first, second, and third neighbors, plus interlayer exchange constant J_z. From these calculations we can extract the values of the exchange constants for different materials, and by comparing the energies of different states we can determine which state would be the ground state for one or the other system.

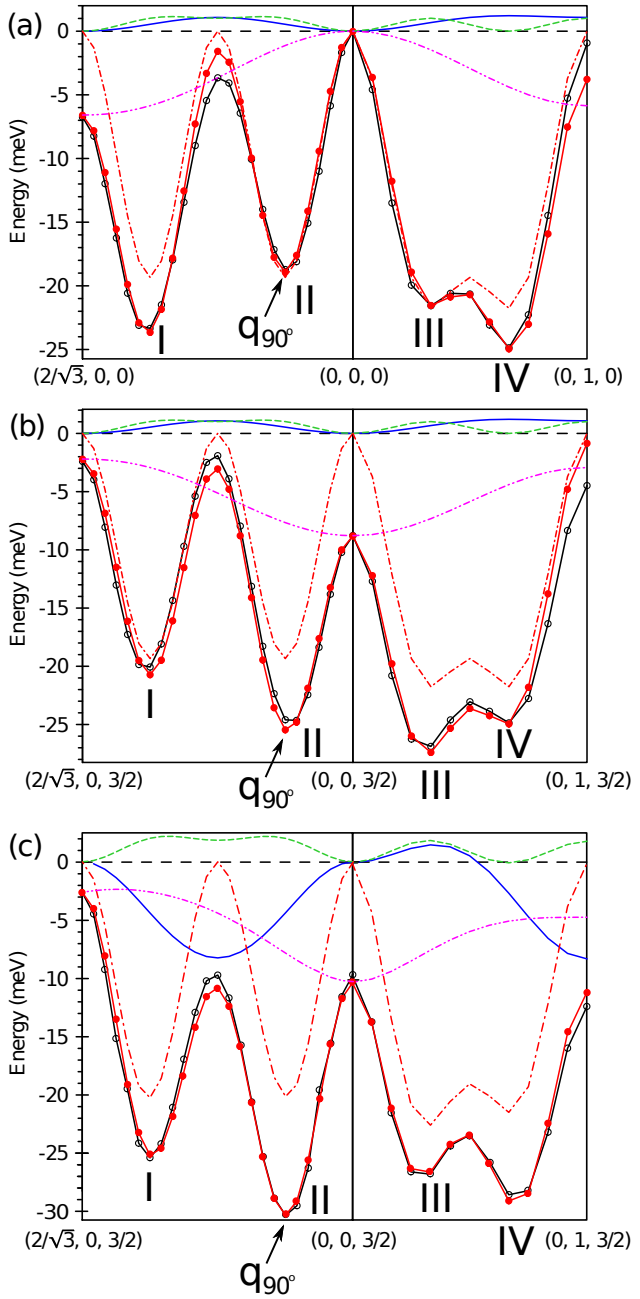

FIG. 4. (Color online) Calculated (open black circles) and fitted (full red circles), using the least-squares method in Heisenberg model, profiles $E(\mathbf{q})$ of magnetic energies for $AgCrS_2$ for two sets of wave vectors, see the text. Partial contributions in magnetic energy, calculated according to (3)–(7), are shown as well. The $\epsilon_1(\mathbf{q})$, $\epsilon_2(\mathbf{q})$, $\epsilon_3(\mathbf{q})$, and $\epsilon_z(\mathbf{q})$ profiles are presented by solid blue, dashed green, dashed with one dot red, and dashed with two dots magenta lines. The dispersion curves shown in panels (a) and (b) are calculated for the high-temperature phase with ferro (a) and antiferro (b) interlayer ordering, whereas those in panel (c) are calculated for the low-temperature structure and antiferro interlayer ordering. The 90° structure, by which we model the double-stripe magnetic structure observed in $AgCrS_2$ and $AuCrS_2$, is marked by arrow.

B. Magnetic structures

Let us discuss the nature of different competing states i.e., different minima of $E(\mathbf{q})$ in Fig. 4. The 120° AFM spin structure observed in $LiCrS_2$ (Ref. 13) is realized by a spin spiral with $\mathbf{q}$=(0,2/3) (in $2\pi/a$ units) which gives the minimum IV in Fig. 4. The local minimum III corresponds to 120° AFM order in the sublattice of 3-rd Cr neighbors.

The FM in-plane structure observed in $KCrS_2$ in Ref. 10 corresponds to $\mathbf{q} = 0$. In contrast, the magnetic energy of $AgCrS_2$ (Fig. 4) has a maximum instead of a minimum at this $\mathbf{q}$ which agrees with the fact that for this system the dominant exchange interactions are antiferromagnetic.

The double-stripe spin structure observed in $AgCrS_2$ cannot be represented as a single $\mathbf{q}$ spiral if the rhombohedral unit cell of the HT $R3m$ structure is used. However, it can be easily verified that the Heisenberg energy of the DS structure is exactly equal to the energy of a spin spiral with $\mathbf{q}_{90°}$=($\sqrt{3}$/6,0), shown by red arrows in Fig. 3, in which spins of each i-th Cr chain running along the y direction turn by 90° with respect to the previous $(i-1)$ one.

Indeed, let us consider the interaction of a Cr spin from some (i=0) chain with the rest of the Cr plane. In the DS structure the spin directions in odd chains to the left $(-2|i|+1)$ and to the right $(2|i|+1)$ are opposite and their contributions to the magnetic energy $J\mathbf{S}_0 \cdot \mathbf{S}_{2|i|+1} = -J\mathbf{S}_0 \cdot \mathbf{S}_{-2|i|+1}$ cancel each other. In the 90° structure odd chains do not contribute to the magnetic energy because of the orthogonality of Cr spins in odd and even chains ($J\mathbf{S}_0 \cdot \mathbf{S}_{2i+1} = 0$). Consequently, the magnetic energy is determined by the interaction of $\mathbf{S}_0$ with $\mathbf{S}_{2i}$ from the even chains which are exactly the same in both spin structures. Here we assume that the exchange coupling constants of $\mathbf{S}_0$ with spins from chains to the left $\mathbf{S}_{-|i|}$ and to the right $\mathbf{S}_{|i|}$ are equal. The couplings between n-th neighbor lying in the same (J_{ny}) and different (J_{nx}) chains need not to be equal so that the degeneracy of the DS and 90° structures holds also for distorted Cr layers of the monoclinic LT phase of $AgCrS_2$.

LSDA supercell calculations performed for the DS and 90° structures also gave the total energies which are equal within the numerical accuracy; with their energy difference being less than 1 meV per Cr ion. Because of the degeneracy of the two spin structures the energy of the DS structure can be calculated within the same spin-spiral approach as the energies of other competing magnetic states. The corresponding energy minimum is marked as II in Fig. 4.

Experimentally, however, these two structures would lead to somewhat different features of neutron scattering spectra although the positions of magnetic Bragg peaks are the same. The authors of [7] concluded that the DS structure better fits the experimental data than the 90° structure.

The same 90° structure within a Cr plane is also real-

ized at $\mathbf{q}$=($3\sqrt{3}$/6,0) corresponding to the minimum I in Fig. 4. However, because of the rather strong interlayer coupling given by Eq. (7) the energies at the minima I and II are not equal. Finally, the maximum at $\mathbf{q}$=($2\sqrt{3}$/6,0) between these two minima corresponds to single-stripe magnetic order, in which FM Cr chains running along y are ordered antiferromagnetically.

Comparing the energies of different states in Fig. 4, we can make several conclusions. First of all, we see that if the ordering between planes would be ferromagnetic and without extra lattice distortion, Fig. 4(a), the absolute minimum for the parameters calculated for $AgCrS_2$ would correspond to the simple 120° AF structure, i.e., the state IV in Fig. 4. Such in-plane ordering is indeed realized in $LiCrS_2$, but for real $AgCrS_2$ the observed ordering is different and corresponds to the double stripe structure.

When we change the interlayer ordering, making it antiferromagnetic, the situation already changes: the 120° state (state IV) is destabilized, and another state, III, becomes the absolute minimum, Fig. 4(b). We also notice that AFM interlayer ordering strongly lowers the energy of the 90° structure (state II in Fig. 4(b)) which, as discussed above, is degenerate with the DS one, so that this state starts to compete with the state III. And when we include the lattice distortion present in $AgCrS_2$ in the LT phase, Fig. 4(c), the double stripe state II becomes the absolute minimum. Thus, we see that for the lattice corresponding to the real LT structure of $AgCrS_2$ the double-stripe magnetic ordering with the antiferromagnetic coupling between layers is indeed the ground state in our calculations. We also see that several factors are important for the stabilization of such DS structure: besides particular ratio of different exchange constants, see below, also particular $3D$ interlayer ordering and lattice distortion, accompanying magnetic ordering, are all important for making double-stripe structure.

But we also see from Fig. 4 that there exist, especially in the HT lattice, other magnetic states competing with the double-stripe one. Thus, one can predict that the magnetic fluctuations above T_N, which could be probed e.g. by inelastic neutron scattering, could be most pronounced not at the wave vector corresponding to the double-stripe ground state structure, but at other values of $\mathbf{q}$, for instance those corresponding to the solutions III and IV in Fig. 4.

Yet one more conclusion which we can extract from Fig. 4 is that, at least in $AgCrS_2$, the spin-lattice (magnetostriction) coupling is very important in these systems: only when we included the lattice distortion, occurring in $AgCrS_2$ below T_N, did we obtain the real double-stripe structure as a ground state.

In addition to the nonrelativistic calculations discussed above, we have also studied the magneto-crystalline anisotropy in $M\mathrm{CrS_2}$ by accounting for spin-orbit coupling in calculations for the FM spin structure with the magnetization directed along different crystallographic axes. It turns out that Cr atoms form an easy-plane magnet, which is consistent with the experimental results:[7,11–14] the spin-orbit coupling rotates all Cr spin magnetic moments into the ab-plane even in high-temperature phase, but does not affect the magnetoelastic in-plane coupling and low-temperature lattice distortion.

C. Exchange constants

The LSDA exchange parameters estimated for the HT structure of all six $M\mathrm{CrS_2}$ compounds by fitting corresponding $E(\mathbf{q})$ using the Heisenberg model defined by (2)–(7) are presented in Table II. We first do not consider the LT phases of $AgCrS_2$ and $AuCrS_2$, because we want to concentrate on general trends observed in this whole class of materials. Detailed results for the LT phases will be presented below. The dependence of the exchange constants on U in LSDA+U calculations will be discussed in Sec. IV E.

From the Table II we see that, with the exception of $AuCrS_2$ which deviates from the general trend and will be discussed below, the variation of the nearest-neighbor exchange J_1 in the series M = Li, Cu, Ag, Na, K clearly correlates with the corresponding structural parameters from Table I. With the increase of the size of M ion and of the Cr–Cr distance, J_1 changes form strongly antiferromagnetic in $LiCrS_2$, with the smallest Li and shortest $d_{\text{Cr-Cr}}$, to strongly ferromagnetic in $KCrS_2$, with the largest K and longest $d_{\text{Cr-Cr}}$, and becomes very small in the Cu and Ag compounds with intermediate Cr–Cr distances.

We also notice that in all the compounds the third neighbor exchange J_3 is antiferromagnetic and rather strong. On the other hand, the second neighbor exchange J_2 is weak and can in most cases be neglected. Apparently it is an interplay of the nn exchange J_1 and the third neighbor exchange J_3 which is primarily responsible for the stabilization of one or the other spin structure in the $M\mathrm{CrS_2}$ series.

TABLE II. Different exchange coupling constants (in meV) in the high-temperature phase of $M\mathrm{CrS_2}$ calculated in LSDA.

M	J_1	J_2	J_3	J_z	J_1/J_3
Li	5.17	0.46	2.73	0.93	1.9
Cu	0.16	0.03	1.51	0.82	0.1
Au	7.41	1.63	5.93	2.93	1.3
Ag	−0.14	−0.13	2.45	0.74	−0.2
Na	−4.06	0.23	2.49	0.09	−1.6
K	−5.45	0.19	2.11	0.05	−2.6

Taking these considerations into account it seems reasonable to apply the J_1–J_3 model to investigate magnetic ordering in $M\mathrm{CrS_2}$. It is well known that the simple J_1 model with antiferromagnetic $J_1 > 0$ (see e.g., Ref. 30) gives noncollinear magnetic ground states with $\mathbf{q} = (0,\ 2/3)$ and angles of 120° between spin magnetic

moments. In the J_1–J_3 model the magnetic energy equals $E_{1,3}(\mathbf{q}) = \epsilon_1(\mathbf{q}) + \epsilon_3(\mathbf{q})$. A simple analysis shows that for positive J_1 and J_3 the wave vector $\mathbf{q}_{\rm IV} = (0, 2/3)$ is still the global minimum with the energy of $E = -3/2(J_1 + J_3)$. Here we consider only extrema at wave vectors lying on x and y axes. Other symmetrically equivalent extrema can be obtained by applying $\pm 2\pi/3$ rotations to corresponding $\mathbf{q}$. The numbering of the minima corresponds to the notations in Fig. 4.

For $|J_1| < 4J_3$ a local minimum appears at $\mathbf{q}_{\rm II} = (q_x, 0)$ on the x axis, with q_x defined by $\cos(\sqrt{3}\pi q_x) = -J_1/4J_3$. When $J_1 < J_3/2$ another minimum $\mathbf{q}_{\rm III}$ appears also on the y axis which becomes the global minimum for FM $J_1 < 0$. If $J_1 = 0$, $\mathbf{q}_{\rm III} = (0,1/3)$ corresponds to 120° order of 3-rd neighbor spins. As the strength of FM J_1 increases, both $\mathbf{q}_{\rm II}$ and $\mathbf{q}_{\rm III}$ shift towards zero, until for FM $|J_1| \geq 4J_3$ the two minima merge at $\mathbf{q} = 0$ which becomes the global minimum.

These additional minima at incommensurate $\mathbf{q}_{\rm II}$ and $\mathbf{q}_{\rm III}$ imply possible formation of helical magnetic order, but the exact picture does depend on interlayer exchange coupling J_z too,[7,14] the latter being one of possible way to stabilize the magnetic structures observed in the "intermediate" systems $M\mathrm{CrS_2}$ (M=Cu, Au, Ag, Na). In particular, this may be the origin of incommensurate magnetic structures for M=Cu, Na, or commensurate double stripes for M=Ag, Au.

An extra complication is introduced by the observed monoclinic distortion in $\mathrm{AgCrS_2}$ and $\mathrm{AuCrS_2}$, which induces three pairs of nonequivalent nearest-neighbor exchange couplings (J_{1x}, J_{1y}), (J_{2x}, J_{2y}), and (J_{3x}, J_{3y}) (see Fig. 3). The observed four-sublattice spin arrangement cancels the effect of J_{1x} and J_{2y}. In order to clarify which of remaining magnetic exchanges are relevant for the stabilization of the DS structure, namely the ferromagnetic first-neighbor coupling J_{1y}, the antiferromagnetic second-neighbor J_{2x} and antiferromagnetic third-neighbors J_{3x} and J_{3y} superexchanges, and the interplane antiferromagnetic superexchange J_z we calculated the energy of different Cr spin moment configurations and derived the corresponding exchange values. The results are summarized in Table III. They show that the monoclinic distortion does stabilize the DS structure by strongly suppressing the AFM contribution to J_{1y} along the FM Cr chains.

TABLE III. LSDA exchange coupling constants (in meV) for low temperature phases of $\mathrm{AgCrS_2}$ and $\mathrm{AuCrS_2}$.

M	J_{1x}	J_{1y}	J_{2x}	J_{2y}	J_{3x}	J_{3y}	J_{zx}	J_{zy}
Au	5.14	2.69	0.70	0.57	3.19	3.24	1.85	1.32
Ag	1.12	−1.36	−0.30	−0.23	2.54	2.62	1.09	0.62

We also have to comment on the values of exchange constants for $\mathrm{AuCrS_2}$ shown in Tables II and III. These values definitely deviate from the regularities observed in other materials of this series. The ratio of the important exchange constants $\mathrm{J_3}$ and $\mathrm{J_1}$ for $\mathrm{AuCrS_2}$ is still such that it gives the double-stripe structure observed experimentally. However the absolute values of these exchanges for this system are about two times larger than what one would expect from the comparison with other materials of this class. We do not have a full explanation of this difference. A possible reason is that $\mathrm{AuCrS_2}$ has a delafossite structure with interlayer $\mathrm{Au^+}$ ions in a linear coordination.[15] It is possible that the reason for different values of exchange for this system is connected with that. Still, this situation is definitely unsatisfactory, and it requires further study.

D. Interpretation of magnetic properties

Our calculations, presented above, have shown that indeed the observed types of magnetic ordering in Cr-plane in $M\mathrm{CrS_2}$ (120° for Li, double stripes for Ag and Au, ferro layers for K) are reproduced. The obtained values of exchange constants, Table II, allow to explain these magnetic structures.

Thus for the smallest M-ion Li the nn exchange J_1 is the strongest and antiferromagnetic; apparently it is predominantly responsible for the observed pure antiferromagnetic (120°) ordering, observed in $\mathrm{LiCrS_2}$. With the increasing of Cr-Cr distance and Cr-S-Cr angle (Li→Cu→Au→Ag→Na→K) the value of J_1 decreases and then changes sign, becoming ferromagnetic for M=Ag, K. Simultaneously the AF exchanges between 3-d neighbors J_3 remains relatively large, and it plays important role for intermediate compounds $\mathrm{Ag/AuCrS_2}$, apparently leading to their double-stripe ordering. Finally, large nearest neighbor ferro interaction J_1 for the large M-ion K guarantees ferro ordering in Cr-plane in $\mathrm{KCrS_2}$.

To understand the microscopic origin of different exchange integrals in this series, one should look at different microscope exchange passes. In Fig. 5(a)-5(d) we show the main paths of superexchange, existing in $\mathrm{CrS_2}$ planes with the $\mathrm{Cr^{3+}}$ ions with d-shell $\mathrm{t_{2g}^3 e_g^0}$ and with the geometry of edge-sharing $\mathrm{CrS_6}$ octahedra with nearest neighbor Cr-S-Cr angle of about 90°.

First of all, there exist a direct overlap of different t_{2g} orbitals of neighboring Cr ions, e.g., xy-orbital in Fig. 5(a). It gives a rather large AF exchange

$$J_a \sim \frac{t_{dd}^2}{U_{dd}}, \tag{9}$$

which however strongly decreases with the increasing of Cr-Cr distance.

In Fig. 5(b) and 5(c) we show an exchange of t_{2g}-t_{2g} via 90° Cr-S-Cr bond. The process 5(b) (virtual hopping of t_{2g} electrons through the same ligand p-orbital, in this case p_z), gives strong AF exchange:

$$J_b \sim \frac{t_{pd\pi}^4}{\Delta^2}\left(\frac{1}{\Delta} + \frac{1}{U_{dd}}\right), \tag{10}$$

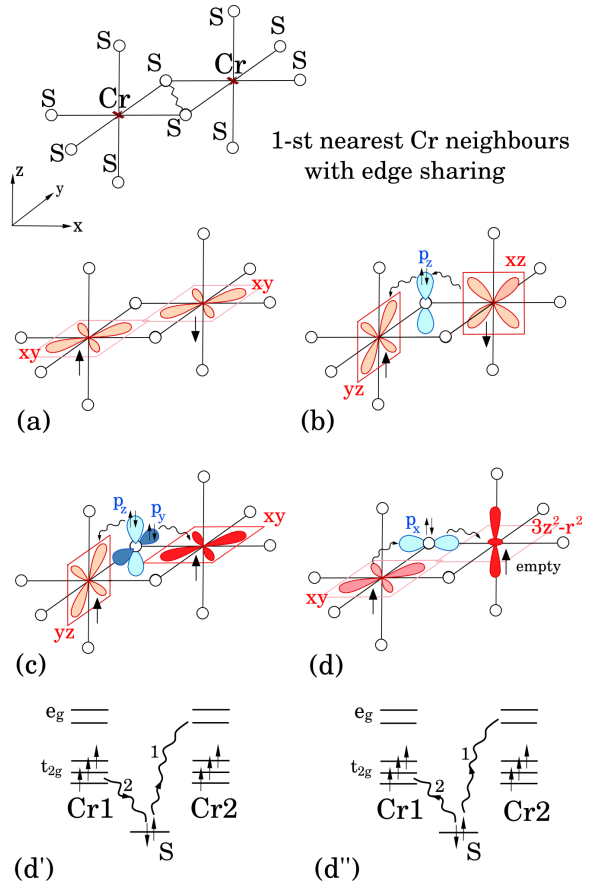

FIG. 5. (Color online) All possible contributions to J_1

where we denoted by Δ the charge-transfer energy (the energy of a transition $Cr^{3+}(d^3)S^{2-}(3p^6) \rightarrow Cr^{2+}(d^4)S^{-}(3p^5)$). One sees that this process does not change strongly with the Cr-S-Cr angle, only the distance Cr-S determines the value of $t_{pd\pi}$ hopping, and this distance is approximately constant in the whole series MCrS$_2$.

The process 5(c) (the t_{2g}-t_{2g} exchanges via different S p-orbitals) leads to the ferromagnetic exchange, which is however usually weaker,

$$J_c \sim -\frac{t_{pd\pi}^4}{\Delta^3} \times \frac{9J_{H,S}}{\Delta}, \qquad (11)$$

(here $J_{H,S}$ is the Hund's rule coupling on sulfur) and it decreases by absolute value with decreasing Cr-S-Cr angle.

More important is another ferromagnetic contribution due to a virtual hopping from the occupied t_{2g}-shell of one Cr to the empty e_g-shells of another Cr, Fig. 5(d). As one sees from Fig. 5(d) this process also gives ferromagnetic contribution,

$$J_d \sim -\frac{t_{pd\sigma}^2 t_{pd\pi}^2}{\Delta^2 U_{dd}} \times \frac{3J_H}{U_{dd}} - \frac{t_{pd\sigma}^2 t_{pd\pi}^2}{\Delta^3} \times \frac{3J_H}{\Delta}, \qquad (12)$$

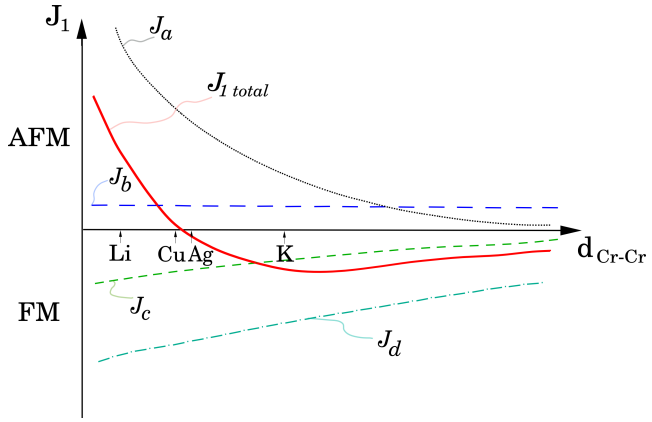

FIG. 6. (Color online) Schematic dependence of different contributions to the nearest neighbor Cr-Cr exchange J_1.

where the first term corresponds to a process 5(d′) (effective transfer of an electron from one Cr to the other via S), and the second 5(d″) (the transfer of two 3p-electrons of S to the left and right Cr ions). We do not keep here some numerical coefficients. Note that despite the presence of a small factors $\frac{J_H}{U_{dd}}$ or $\frac{J_H}{\Delta}$, this ferromagnetic contribution (12) is comparable with (9) (typically $t_{pd\sigma} \sim \sqrt{2}t_{pd\pi}$), and also the Hund's rule contribution in (12) is enhanced by factor 3. Thus, though usually the 90°-exchange involving Hund's rule interaction gives ferromagnetic, but weaker exchange, in this case due to a specific electrons occupation of Cr^{3+} it can give significant contribution and can even start to dominate if the other competitive contributions are small. This is apparently what happens in KCrS$_2$, in which the main competing AF exchange 5(a) is strongly reduced due to a large size of K^+ and corresponding increase of Cr-Cr distance.

Thus, we can schematically present different contributions to the nearest neighbor exchange J_1 and their change in the row (Li→Cu→Au→Ag→Na→K)CrS$_2$ as following, Fig. 6.

To explain the resulting magnetic structures, especially double-stripe structure of AuCrS$_2$ and AgCrS$_2$, we also have to include the further neighbor exchange. As seen from Table II, the second neighbor exchange is always small. Somewhat surprisingly, larger and more important turns out to be the interaction of third neighbors. It can be schematically explained by the consideration shown in Fig. 7, in which one sees that there is an exchange path connecting occupied t_{2g} orbitals on third neighbors Cr$_1$ and Cr$_3$ via two sulfur S$_1$ and S$_2$, (with their p-orbitals being relatively large) due to the p-p overlap, or to the overlap via an empty e_g-orbital (x^2-y^2) of Cr$_2$ (Fig. 7).

Thus in this geometry the coupling between third neighbors J_3 turns out to be reasonably large (larger than J_2) and antiferromagnetic, and in effect it is this coupling which stabilizes double-stripe structure for "intermediate" composition AgCrS$_2$ and AuCrS$_2$, in which the main nearest neighbor interaction J_1 is small due to

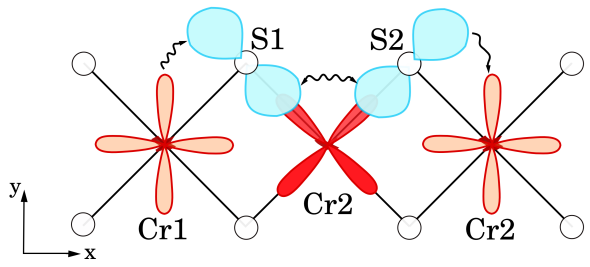

FIG. 7. (Color online) A possible exchange path contributing to the antiferromagnetic exchange of third neighbors J_3.

a compensation of different contributions to it.

The general tendency showing regular change of different exchange contributions, especially of the nearest neighbor exchange J_1, see Fig. 6, is also confirmed by model calculations in which we took $LiCrS_2$ and artificially compressed it in c-direction, keeping the volume constant. At this change the in-plane Cr-Cr distance and Cr-S-Cr angle increase, following the same trends as in going from $LiCrS_2$ to (Ag, Au) and to $KCrS_2$. Our *ab-initio* calculations of this model system confirmed the trend discussed above: with increasing Cr-Cr distance large AF coupling J_1 strongly decreases and becomes ferromagnetic.

E. The effect of LSDA+U on calculated exchange constants

So far we discussed only exchange coupling constants determined by fitting $E(\mathbf{q})$ curves calculated within LSDA (Table II). Comparing the J_1/J_3 ratio from Table II with the critical values obtained from the analysis of the J_1–J_3 Heisenberg model one notices that for some of the compounds the estimated J_i do not give an experimentally observed ground state. For $KCrS_2$, for example, $J_1/J_3 = -2.6 > -4$ corresponds to an incommensurate spin-spiral structure in the a-b plane instead of experimental FM ordering.

One of possible reasons for this is that the LSDA underestimates the Coulomb repulsion between rather localized Cr $3d$ electrons. The U_{dd} parameter in expressions (9)–(12) is the energy cost of adding an electron to one of the unoccupied minority-spin t_{2g} state. In LSDA it is governed solely by the exchange splitting of about 2.4 eV between the minority- and majority-spin t_{2g} states, i.e., by Hund's coupling of $3J_H$. As a result the LSDA overestimates those contributions to the inter-site exchanges that have U_{dd} in the denominator. Accounting for the Coulomb repulsion in LSDA+U calculations increases the energy difference between the minority- and majority-spin Cr t_{2g} states by $U_{\rm eff}$, so that U_{dd} becomes equal $3J_H + U_{\rm eff}$.

The increase of $U_{\rm eff}$ suppresses AFM J_a and J_b, whereas the FM t_{2g}–e_g contribution J_d is much less affected. Thus, in the compounds with FM J_1 (M = Na, K) it becomes even stronger, whereas in those compounds for which LSDA gives AFM J_1 its value decreases and it may even change sign. On the other hand, the AFM 3-rd neighbor coupling J_3, which is governed by the t_{2g}–t_{2g} superexchange (Sec. IV D), gradually decreases with the increase of $U_{\rm eff}$.

This combined effect of strengthening the FM J_1 and weakening the AFM J_3 leads to a reduction in the J_1/J_3 ratio estimated for $KCrS_2$ from -2.6 in LSDA to -4.6 and -6.4 in LSDA+U calculations with $U_{\rm eff} = 1$ and 2 eV, respectively. Thus, accounting for Coulomb repulsion stabilizes the FM in-plane order in $KCrS_2$. In $LiCrS_2$ the 120° structure gives the lowest total energy also in LSDA+U calculations. In other compounds the increase of $U_{\rm eff}$ changes the J_1/J_3 ratio and, consequently, the position of incommensurate minima.

V. SUMMARY

Summarizing, the results of our *ab-initio* calculations, and model considerations of Sec. IV D allowed us to explain the very interesting sequence of magnetic phases in layered chromites $MCrS_2$ with triangular Cr layers, in which the magnetic ordering in Cr layers changes from purely antiferromagnetic (120°) structure in $LiCrO_2$ via "intermediate" double-stripe structure of $AgCrS_2$ and $AuCrS_2$ (and incommensurate structure in $NaCrS_2$ and $CuCrS_2$) to a ferromagnetic layers in $KCrS_2$. These structures emerge mainly as a result of competing contributions to the nearest neighbor exchange J_1, together with reasonably large antiferromagnetic exchange for third neighbors J_3. In particular, their combined action leads to the most interesting double stripe structure of $AuCrS_2$ and $AgCrS_2$, which apparently is responsible for the multiferroic behavior of the latter (and probably also in the former — it is not checked yet). Our study demonstrates quite nontrivial interplay of lattice geometry and orbital occupation in giving such diverse magnetic behavior in apparently rather similar materials. The frustrated nature of the lattice definitely plays a very important role in these phenomena. Such high sensitivity of magnetic, and apparently some other, e.g., multiferroic properties to fine details of electronic and lattice structure could probably be used also to tune the properties of other similar materials. We envisage that further studies of the stability of nuclear and magnetic structures may provide a clue to tailor the magnetoelastic coupling and the multiferroic properties in geometrically frustrated oxides, sulfides and selenides with different transition metals.

ACKNOWLEDGMENTS

A. V. Ushakov and D. A. Kukusta gratefully acknowledge the hospitality at Max-Planck-Institut für Festkörperforschung in Stuttgart during their stay there.

The authors are grateful to S. Hebert and C. Martin for discussion of experimental situation. The work of A. U. and D. Kh. was supported by the European program SOPRANO and by the German projects SFB 608 and FOR 1346.

[1] A. P. Ramirez, Annu. Rev. Mater. Sci. **24**, 453 (1994)
[2] M. F. Collins and O. A. Petrenko, Can. J. Phys. **75**, 605 (1997)
[3] K. Koumoto, I. Terasaki, and R. Funahashi, MRS Bulletin **31**, 206 (2006)
[4] D. I. Khomskii, Physics (Trends) **2**, 20 (2009)
[5] S.-W. Cheong and M. Mostovoy, Nature Materials **6**, 13 (2007)
[6] M. Poienar, C. Vecchini, André, A. Paoud-Aladine, I. Margiolaki, A. Maignan, A. Lappas, L. Chapon, M. Hervieu, F. Damay, and C. Martin, Chem. Mater. **23**, 85 (2011)
[7] F. Damay, C. Martin, V. Hardy, G. Andre, S. Petit, and A. Maignan, Phys. Rev. B **83**, 184413 (2011)
[8] A. M. K. Singh, C. Martin, and C. Simon, Physical Inogranic Chemistry **41**, 4 (2010)
[9] L. K. Alexander, N. Büttgen, R. Nath, A. V. Mahajan, and A. Loidl, Phys. Rev. B **76**, 064429 (2007)
[10] B. van Laar and F. M. R. Engelsman, J. Solid State Chem. **6**, 384 (1973)
[11] W. Rüdorff and K. Stegemann, Zeitschrift für anorganische und allgemeine Chemie **251**, 376 (1943)
[12] F. M. R. Engelsman, G. A. Wiegers, F. Jellinek, and B. van Laar, J. Solid State Chem. **6**, 574 (1973)
[13] B. van Laar and D. J. W. Ijdo, J. Solid State Chem. **3**, 590 (1971)
[14] S. J. E. Carlsson, G. Rousse, I. Yamada, H. Kuriki, R. Takahashi, F. Levy-Bertrand, G. Giriat, and A. Gauzzi, Phys. Rev. B **84**, 094455 (2011)
[15] A. Pabst, American Mineralogist **31**, 539 (1946)
[16] A. Lafond, W. Henggeler, H. Mutka, and B. Ouladdiaf, Can. J. Phys. **79**, 11 (2001)
[17] D. I. Khomskii, J. Magn. Magn. Mater **306**, 1 (2006)
[18] O. K. Andersen, Phys. Rev. B **12**, 3060 (1975)
[19] A. Perlov, A. Yaresko, and V. Antonov, "Py-lmto, a spin-polarized relativistic linear muffin-tin orbitals package for electronic structure calculations," "PY-LMTO, A Spin-polarized Relativistic Linear Muffin-tin Orbitals Package for Electronic Structure Calculations", unpublished.
[20] J. Perdew and Y. Wang, Phys. Rev. B **45**, 13244 (1992)
[21] P. Blöchl, O. Jepsen, and O. K. Andersen, Phys. Rev. B **49**, 16223 (1994)
[22] L. M. Sandratskii, J. Phys.: Condens. Matter **3**, 8565 (1991)
[23] A. N. Yaresko, A. Y. Perlov, R. Hayn, and H. Rosner, Phys. Rev. B **65**, 115111 (2002)
[24] A. N. Yaresko, Phys. Rev. B **77**, 115106 (2008)
[25] L. R. Mackintosh and O. K. Andersen, in *Electrons at the Fermi Surface*, edited by M. Springford (Cambridge University Press, Cambridge, England, 1980)
[26] W. E. Pickett, A. J. Freeman, and D. D. Koelling, Phys. Rev. B **22**, 2695 (1980)
[27] V. I. Anisimov, F. Aryasetiawan, and A. I. Liechtenstein, J. Phys.: Condens. Matter **9**, 767 (1997)
[28] M. T. Czyżyk and G. A. Sawatzky, Phys. Rev. B **49**, 14211 (1994)
[29] A. N. Yaresko, V. N. Antonov, and P. Fulde, Phys. Rev. B **67**, 155103 (2003)
[30] A. L. Chernyshev and M. E. Zhitomirsky, Phys. Rev. B **79**, 144416 (2009), and references therein.